J|A|C|S ARTICLES

Published on Web 04/09/2009

Theoretical Study of the Chemiluminescent Decomposition of Dioxetanone

Fengyi Liu,[†] Yajun Liu,*[,‡] Luca De Vico,[†,§] and Roland Lindh*[,†]

Department of Theoretical Chemistry, Lund University, Chemical Center, P.O. Box 124, SE-221 00 Lund, Sweden, and College of Chemistry, Beijing Normal University, Beijing 100875, P. R. China

Received October 29, 2008; E-mail: yajun.liu@bnu.edu.cn; roland.lindh@teokem.lu.se

Abstract: The unimolecular chemiluminescent decomposition of unsubstituted dioxetanone was studied at the complete active space self-consistent field level of theory combined with the multistate second-order multiconfigurational perturbation theory energy correction. The calculations revealed interesting features. Two transition states, two conical intersections, and one intermediate stable biradical structure along the lowest energy reaction path were identified. It was noted that the conical intersections are found at or in very close proximity to the transition states. The first and second transition states correspond to O−O and C−C cleavages, respectively. In particular, a planar structure is supported by the $^1(\sigma,\sigma^*)$ state during the O−O dissociation up to the first transition state and conical intersection. At this point the $^1(\sigma,\sigma^*)$ state dissociation path bifurcates, corresponding to a torsion of the O−C−C−O angle. Simultaneously, the $^1(n,\sigma^*)$ state becomes lower in energy while still favoring a planar structure. As the lowest-energy reaction path proceeds toward the second transition state and conical intersection, the $^1(n,\sigma^*)$, $^3(n,\sigma^*)$, and $^1(\sigma,\sigma^*)$ states are close in energy. This work suggests that the vibrational distribution at the first conical intersection and the interactions among the states as the reaction proceeds between the two transition states are the origin of the population of the chemiluminescent (n,σ^*) states.

1. Introduction

Bioluminescence, the emission of light by living organisms, is undoubtedly one of the wonders of nature.[1] Anybody who has seen such a magical phenomenon cannot help asking "How does it work?" Thanks to the joint efforts of biologists and chemists, we now know that a class of chemical reactions is responsible for the light-emission process in bioluminescent creatures.[2] Usually these reactions involve the formation and decomposition of a family of four-membered-ring peroxides, namely, 1,2-dioxetanes (Chart 1). For instance, the mechanism of the most efficient bioluminescent system, firefly luminescence,[3,4] can be described as follows: In the presence of the enzyme luciferase, the firefly luciferin pigment is initially oxidized to produce a high-energy carbonyl dioxetane (firefly dioxetanone, Chart 1). This is followed by a two-step event, (1) the rupture of the weak peroxide bond and (2) the dissociation of the

Chart 1

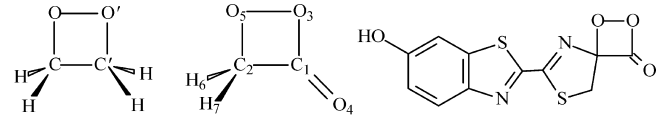

associated carbon−carbon bond, resulting in a carbonyl-containing molecule (oxyluciferin) in an excited state. Finally, the excited-state oxyluciferin decays to the ground state with emission of light. Without any doubt, detailed information about the adiabatic potential energy surfaces (PESs) and in-depth knowledge of the reaction mechanism of dioxetanones are the prerequisites for understanding the chemical nature of complicated bioluminescent systems and developing novel high-efficiency chemiluminescent substrates.[2b]

Although firefly luminescence has attracted much experimental[5] and theoretical attention,[6] the complete details of this enzyme-catalyzed reaction involving dioxetanones, especially of the key step relating to generation of the excited state, still have not been completely explored. This is due to experimental obstacles (such as difficulties in synthesis, low thermal and

[†] Lund University.
[‡] Beijing Normal University.
[§] Present address: Department of Chemistry, University of Copenhagen, Universitetsparken 5, DK-2100, Copenhagen, Denmark.

(1) (a) *Bioluminescence and Chemiluminescence*; Kaplan, N. P., Colowick, N. P., DeLuca, M. A., Eds.; Methods in Enzymology, Vol. 57; Academic Press: New York, 1978. (b) *Chemical and Biological Generation of Excited States*; Adam, W., Cilento, G., Eds.; Academic Press: New York, 1982.
(2) (a) Hastings, J. W. *J. Mol. Evol.* **1983**, *19*, 309. (b) Matsumoto, M. *J. Photochem. Photobiol., C* **2004**, *5*, 27.
(3) McCapra, F.; Chang, Y. C.; Francois, V. P. *Chem. Commun.* **1968**, 22.
(4) (a) White, E. H.; Rapaport, E.; Seliger, H. H.; Hopkins, T. A. *J. Am. Chem. Soc.* **1969**, *91*, 2178. (b) White, E. H.; Rapaport, E.; Seliger, H. H.; Hopkins, T. A. *Bioorg. Chem.* **1971**, *1*, 92. (c) Shimomura, O.; Goto, T.; Johnson, F. H. *Proc. Natl. Acad. Sci. U.S.A.* **1977**, *74*, 2799.
(5) (a) White, E. H.; Miano, J. D.; Umbreit, M. *J. Am. Chem. Soc.* **1975**, *97*, 198. (b) White, E. H.; Steinmetz, M. G.; Miano, J. D.; Wildes, P. D.; Morland, R. *J. Am. Chem. Soc.* **1980**, *102*, 3199. (c) Ugarova, N. N.; Brovko, L. Y. *Luminescence* **2002**, *17*, 321. (d) Branchini, B. R.; Magyar, R. A.; Murtiashaw, M. H.; Portier, N. C. *Biochemistry* **2001**, *40*, 2410. (e) Branchini, B. R.; Murtiashaw, M. H.; Magyar, R. A.; Portier, N. C.; Ruggiero, M. C.; Stroh, J. G. *J. Am. Chem. Soc.* **2002**, *124*, 2112.

catalytic stabilities, etc.)[7] as well as the following theoretical challenges. In order to deal with such nonadiabatic chemiluminescent reactions, where more than two states are involved, state-specific single-reference methods are insufficient, as are some multireference treatments that do not take into account an adequate number of states. For instance, our recent calculations on the thermal decomposition of 1,2-dioxetane showed that a multistate complete active space second-order perturbation theory (CASPT2)[8] treatment based on a four-root state-average reference wave function is indispensably required.[9] This was true when fully describing the reaction route and especially when characterizing the regions where the adiabatic excited-state surfaces are strongly coupled with the ground state. Moreover, a rational mechanistic study at the complete active space self-consistent field (CASSCF)[10] level must include in the active space electrons and orbitals from both the dioxetanone and heterocyclic moieties; unfortunately, to date the size of firefly dioxetanone has prevented a high-level calculation. Although a recent theoretical attempt to elucidate the mechanism of firefly chemiluminescence was reported,[6d] their exclusion from the active space of the lone pairs on oxygen in the dioxetanone moiety placed their PESs as well as the suggested overall mechanism into question. It is known from simple dioxetane[9] and dioxetanone systems (see section 3) that the excited-state chemiluminescent product results from an $n \rightarrow \sigma^*$ transition of these lone pairs. Thus, an active space including these lone-pair orbitals and electrons is a prerequisite for the CASSCF calculation. Although the origin of the chemiluminescence in larger substituted dioxetanone systems is expected to be more complicated and in some cases the electronic transition from the heterocyclic moiety may be more important, one cannot exclude the contribution of the inherited $n \rightarrow \sigma^*$ transition mode without strong experimental evidence. Actually, even for the "simplest" alkyl-substituted dioxetanones, which represent the basic model of firefly luciferin, the chemiluminescence process is not fully understood. The very few theoretical calculations concerning the decomposition of the simplest dioxetanones do not possess sufficient quantitative and qualitative accuracy.[11] The state-averaged CASSCF (SA-CASSCF) calculation by Chung et al.[6d] failed to identify two key conical intersections and thus was unable to rationalize the reaction mechanism (see the Supporting Information for ref 6d). Before the peak of full understanding of the light-generation process in fireflies can be conquered, the PESs and detailed mechanism of the chemiluminescent decomposition of simple dioxetanone must be clearly understood. Thus, we initiated a theoretical investigation of the mechanism of the unimolecular decomposition of unsubstituted dioxetanone (Chart 1).

Our knowledge concerning the chemiluminescence of alkyl dioxetanones originates from the pioneering work of Adam and co-workers.[7] In 1972, Adam and Liu[7a] reported the synthesis of the first alkyl dioxetanone, *tert*-butyldioxetanone, which was found to generate a carbonyl product and emit light via unimolecular thermal fragmentation. Thereafter, experimental studies of the thermolysis of dimethyldioxetanone in solution were carried out by Schuster's[12] and Turro's groups.[13] The fundamental data, such as the quantum efficiencies and activation parameters, including the activation energy corresponding to the thermal disappearance of reactant (E_a) and the chemiluminescence-intensity activation energy (E_{chl}) resulting from the formation of singlet acetone, were reported. The E_a measured by Schmidt and Schuster in $C_2Cl_3F_3$ solution (22.3 ± 0.6 kcal mol^{-1})[12] is approximately identical to that obtained by Turro and Chow in $CFCl_3$ solution.[13] However, the E_{chl} values reported by these authors, 25.6 ± 0.1 and 21.6 ± 0.8 kcal mol^{-1}, respectively, are inconsistent with each other. This discrepancy voided a conclusive identification of the reaction mechanism, i.e., discrimination between a stepwise or a concerted mechanism. High-level theoretical calculations can assist in such an assessment. The main purpose of this study was to reveal the true nature of the mechanism and quantitatively predict these activation energies for the thermal decomposition of dioxetanone in the gas phase.

2. Computational Details

The geometries of the reactant, transition states, and possible intermediates on the ground state (S_0), first singlet state (S_1), and triplet state (T_1) PESs were optimized at the two-root equal-weights SA-CASSCF[10] level of theory with no symmetry constraints. The SA-CASSCF model allows for a balanced description of the lowest two singlet and triplet states. Here the two-root SA-CASSCF wave functions are adequate for the following reason: Unlike the thermal decomposition of 1,2-dioxetane, in which the two formaldehyde moieties have equal chances to be excited (giving a total of four couplings of these states),[9] the decomposition of dioxetanone produces only formaldehyde in an excited state, while the carbon dioxide is always found in the ground state.[12,13] Therefore, only the two lowest states are involved in the reaction; in addition, the higher states were found to have only a minor influence on the two lowest states. The double-ζ ANO-RCC[14] basis sets with a contraction scheme [3s2p1d] for carbon and oxygen atoms and [2s1p] for hydrogen (i.e., the ANO-RCC-VDZP basis sets) were used in geometry optimizations. The pathways linking the stationary points and the hypersurface crossings were verified by minimum-energy path (MEP) searches.[15] The MEP was in all cases established on the lowest-state surface, except in the case of the final dissociation channels, where MEPs on both the ground- and excited-state surfaces were computed. Vibrational frequencies were calculated at the same level using a numerical method in order to get zero-point energies (ZPE). The branching space at the conical intersection (CI) was computed numerically.[16]

The energies of the optimized geometries were reevaluated at the multistate CASPT2 (MS-CASPT2)[8] level of theory using the triple-ζ ANO-RCC basis sets ([4s3p2d1f] for C and O and [3s2p1d] for H, denoted as the ANO-RCC-VTZP basis sets). To precisely

(6) (a) Orlova, G.; Goddard, J. D.; Brovko, L. Y. *J. Am. Chem. Soc.* **2003**, *125*, 6962. (b) Isobe, H.; Takano, Y.; Okumura, M.; Kuramitsu, S.; Yamaguchi, K. *J. Am. Chem. Soc.* **2005**, *127*, 8667. (c) Nakatani, N.; Hasegawa, J.; Nakatsuji, H. *J. Am. Chem. Soc.* **2007**, *129*, 8756. (d) Chung, L. W.; Hayashi, S.; Lundberg, M.; Nakatsu, T.; Kato, H.; Morokuma, K. *J. Am. Chem. Soc.* **2008**, *130*, 12880.
(7) (a) Adam, W.; Liu, J.-C. *J. Am. Chem. Soc.* **1972**, *94*, 2894. (b) Adam, W.; Simpson, G. A.; Yany, F. *J. Phys. Chem.* **1974**, *78*, 2559.
(8) Finley, J.; Malmqvist, P.-Å.; Roos, B. O.; Serrano-Andrés, L. *Chem. Phys. Lett.* **1998**, *288*, 299.
(9) De Vico, L.; Liu, Y.-J.; Krogh, J. W.; Lindh, R. *J. Phys. Chem. A* **2007**, *111*, 8013.
(10) Roos, B. O. In *Ab Initio Methods in Quantum Chemistry II*; Lawley, K. P., Ed.; Advances in Chemical Physics, Vol. 69; John Wiley & Sons: New York, 1987; pp 399−446.
(11) (a) Schmidt, S. P.; Vincent, M. A.; Dykstra, C. E.; Schuster, G. B. *J. Am. Chem. Soc.* **1981**, *103*, 1292. (b) Kasney, M.; Pamuk, H. O.; Trindle, C. *THEOCHEM* **1983**, *104*, 459. (c) Wada, N.; Sakai, H. *J. Biol. Phys.* **2005**, *31*, 403.
(12) (a) Schmidt, S. P.; Schuster, G. B. *J. Am. Chem. Soc.* **1978**, *100*, 5559. (b) Schuster, G. B.; Schmidt, S. P. *J. Am. Chem. Soc.* **1980**, *102*, 306.
(13) Turro, N. J.; Chow, M.-F. *J. Am. Chem. Soc.* **1980**, *102*, 5058.
(14) Roos, B. O.; Lindh, R.; Malmqvist, P.-Å.; Veryazov, V.; Widmark, P.-O. *J. Phys. Chem. A* **2004**, *108*, 2851.
(15) De Vico, L.; Olivucci, M.; Lindh, R. *J. Chem. Theory Comput.* **2005**, *1*, 1029.

Chart 2

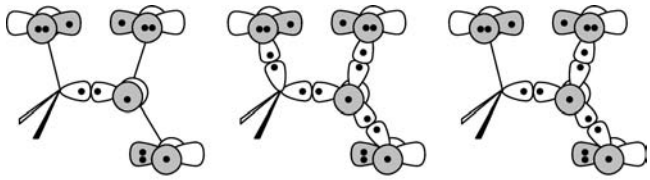

calculate the activation energies, some structures were directly optimized on the MS-CASPT2 PES, and a numerical method was employed in calculating the energy gradients. In all of the MS-CASPT2 calculations, the core orbitals of non-hydrogen atoms were not correlated, and the standard IPEA modification of the zeroth-order Hamiltonian with a value of 0.25 was employed.[17]

The selection of a reasonable active space was unexpectedly tricky. Ideally, the "minimal" active space of 12 electrons distributed in nine orbitals [denoted as CAS(12-in-9); see Chart 2] should be an optimal candidate for the calculation along the whole reaction path. Unfortunately, our preliminary calculations were found to be unstable as a result of strong interactions among the C_1-C_2, C_1-O_3, and C_1-O_4 σ bonding and antibonding orbitals. During the reaction path, the characters of these three bonds were repartitioned. Thus, it was impossible to separate one from the others. However, selection of the CAS(18-in-15) active space (Chart 2), which includes all of the bonding/antibonding orbitals and the lone pairs of the non-hydrogen atoms, would have caused the corresponding calculation to become prohibitive. Finally, an active space of 16 electrons in 13 orbitals [CAS(16-in-13); Chart 2] was chosen. The set of active orbitals comprises the C−C, O−O, and C−O (except for C_2-O_5) bonding and antibonding orbitals plus the lone-pair orbitals of the three oxygens. The exclusion of the C_2-O_5 σ/σ^* orbitals and electrons from the CASSCF active space should have less influence on the final result than the exclusions for the CAS(12-in-9) active space. Preliminary calculations revealed that the nature of these two orbitals would remain more or less intact during the reaction process. Along the reaction path, the O−O and C−C bond breakage causes some σ/σ^* orbitals to change nature and become first lone pairs and then π/π^* orbitals in the CH_2O and CO_2 moieties.

All of the calculations were performed using the MOLCAS 7.0 suite of programs.[18]

3. Results and Discussion

Before the details of the reaction are discussed, an analysis of the electronic structure of dioxetanone would be helpful. The ground state of dioxetanone is dominated by a closed-shell Hartree−Fock configuration with all bonding- and lone-pair orbitals being doubly occupied, while the S_1 and T_1 states result from an $n \rightarrow \sigma^*$ transition from the perpendicular lone-pair orbital of O_5 to the O−O σ^* orbital. As the peroxide bond gradually becomes elongated, the O−O σ and σ^* orbitals become more and more degenerate, with the result that the ground-state transition state (TS) shows a (σ,σ^*) character. Thus, the initial ground-state PES can essentially be described as the $^1(\sigma,\sigma^*)$ surface, and the S_1 and T_1 states are assigned as the $^1(n,\sigma^*)$ and $^3(n,\sigma^*)$ states, respectively. After the dissociation of the C−C bond, carbon dioxide (CO_2) is formed in the ground state and formaldehyde (CH_2O) in the S_0, S_1, and T_1 states.

The detailed results of our calculations are presented in the following sections. First, the SA-CASSCF-optimized geometries of the stationary points on the ground- and excited-state PESs and the activation energies obtained at various levels of theory are shown in section 3.1. In section 3.2, the MEP over the ground-state $^1(\sigma,\sigma^*)$ surface calculated at the MS-CASPT2//SA-CASSCF level of theory is presented. This corresponds to the reaction path starting from the reactant and ending at the first conical intersection, namely, the **$^1(\sigma,\sigma^*)$-Min−TS-1−CI-1** MEP. Next, section 3.3 discusses the MEPs over the $^1(n,\sigma^*)$ and $^3(n,\sigma^*)$ excited-state surfaces, emphasizing in particular the region between the first and second CIs where the ground and excited adiabatic states intersect. Finally, in section 3.4, a reaction coordinate analysis is presented, after which a possible mechanism is proposed.

3.1. Optimized Geometries and Activation Energies. The geometric parameters of the minima and transition states on the ground (S_0), first singlet (S_1), and triplet (T_1) states as well as the state-crossing points are presented in Table 1. It is worth noting that all of the optimized geometries are effectively planar. This contrasts with the decomposition of 1,2-dioxetanes (Chart 1), for which the O−C−C′−O′ dihedral angle of the molecule gradually increases along the reaction path. Furthermore, the corresponding torsional mode in 1,2-dioxetane was suggested to be responsible for the formation of a particular entropic trapping process[19] that played a central role in producing excited-state species as well as regulating the ratio of excited- to ground-state products.[9] This difference results from the conjugation effect in the planar dioxetanone, which more or less restricts the torsion around C−C bond during motion along the reaction path. Hence, the decomposition of dioxetanone is expected to exhibit some distinctive characteristics as compared with 1,2-dioxetane.

Table 1 also presents the relative energies of the optimized geometries calculated at the MS-CASPT2 level. The decomposition barrier corresponding to the thermal decomposition of reactant (E_a) is 28.6 kcal mol^{-1}. With ZPE correction, the height

(16) The branching space at the CI was established as follows: (1) The analytic energy gradients of the two states were computed for the reference CI structure and for a set of structures corresponding to positive and negative Cartesian displacements of ±0.01 and ±0.05 au around this reference structure. (2) An energy difference function, $G = (E_0 - E_1)^2$, was assumed to be approximated to a quadratic function around the reference CI structure. (3) The analytic Cartesian gradients of G were easily constructed from the energies and analytic energy gradients of the two states. (4) The second-order derivative matrix was constructed numerically by the use of a two-point symmetric formula. (5) The branching vectors were established as the two leading vectors when the second-order derivative matrix was subjected to a reduced Cholesky decomposition. The consistency of the resulting vectors was established by comparing the vectors obtained using the two differently sized displacements.

(17) Ghigo, G.; Roos, B. O.; Malmqvist, P.-Å. *Chem. Phys. Lett.* **2004**, *396*, 142.

(18) (a) Andersson, K.; et al. *MOLCAS*, version 7.0; Lund University: Lund, Sweden, 2007. (b) Karlström, G.; Lindh, R.; Malmqvist, P.-Å.; Roos, B. O.; Ryde, U.; Veryazov, V.; Widmark, P.-O.; Cossi, M.; Schimmelpfennig, B.; Neograd, P.; Seijo, L. *Comput. Mater. Sci.* **2003**, *28*, 222. (c) Veryazov, V.; Widmark, P.-O.; Serrano-Andrés, L.; Lindh, R.; Roos, B. O. *Int. J. Quantum Chem.* **2005**, *100*, 626.

(19) The entropic trap effect, which is exclusive to multidimensional PESs, acts effectively as if there is a local energy minimum on the PES although no such minimum is present. The effect occurs in cases where the PES is bound in several dimensions but open in only one or a few directions. A molecule that enters such a region with its vibrational modes mainly populating the bound dimensions is forced to spend some time in the entropic trap to redistribute the vibrational mode populations in order to access the dimensions on the PES that are not bound. The time spent in the trap can in some cases be of such a magnitude that it can mistakenly be interpreted as the presence of a true local minimum. An example of this in chemistry is documented in the dissociation of cyclobutane as studied by Zewail and co-workers (see: Pedersen, S.; Herek, J. L.; Zewail, A. H. *Science* **1994**, *266*, 1359; Polanyi, J. C.; Zewail, A. H. *Acc. Chem. Res.* **1995**, *28*, 119.). The entropic trapping effect becomes more pronounced as the dimensionality of the PES increases.

Table 1. Geometrical Parameters, Relative Energies, and Energy Gaps of Important Geometries on the Ground and Excited States at the MS-CASPT2//SA-CASSCF Level of Theory

	$^1(\sigma,\sigma^*)$-Min	$^1(\sigma,\sigma^*)$-TS	$^1(n,\sigma^*)$-Min	$^1(n,\sigma^*)$-TS	$^3(n,\sigma^*)$-Min	$^3(n,\sigma^*)$-TS	CI-1 (ISC-1)	$^1(n,\sigma^*)$-TS′ CI-2 (ISC-2)[a]
				Bond Lengths (Å)				
C_1-C_2	1.507	1.506	1.514	1.674	1.512	1.665	1.507	1.602
O_3-O_5	1.577	2.455	2.692	2.688	2.678	2.702	2.488	2.702
C_2-O_5	1.415	1.385	1.372	1.355	1.373	1.350	1.385	1.368
C_1-O_3	1.386	1.334	1.330	1.265	1.330	1.273	1.333	1.309
C_1-O_4	1.191	1.214	1.219	1.208	1.219	1.207	1.216	1.209
				Bond Angles (deg)				
$C_1-C_2-O_5$	89.7	106.5	114.6	119.2	114.3	119.8	107.3	119.9
$O_3-C_1-C_2$	93.2	114.5	117.1	106.2	116.8	106.8	115.2	107.0
$O_3-C_1-O_4$	127.0	117.4	117.7	138.7	117.7	137.2	117.2	135.9
				Relative Energies (kcal mol^{-1})[b]				
SA-CASSCF	0.0	11.7	9.9	18.8	9.7	17.0	11.8 (11.4)	15.7 (15.2)
MS-CASPT2	0.0	28.6	27.9	24.9	28.3	27.1	29.5 (29.6)	30.4 (31.2)
				S_1-S_0 (T_1-S_0) Gaps (kcal mol^{-1})				
SA-CASSCF	91.2	1.0	−4.0	7.5	−4.0	4.3	0.0 (−0.4)	−2.3 (−2.8)
MS-CASPT2	83.3	1.6	−4.3	9.1	−3.8	9.1	0.6 (0.7)	−2.6 (−1.8)

[a] Nonoptimized geometry obtained from the MS-CASPT2//SA-CASSCF-predicted $^1(n,\sigma^*)$ MEP curve at reaction coordinate ≈ −0.05 au. [b] Energies relative to the S_0 energy of **$^1(\sigma,\sigma^*)$-Min**.

Table 2. MS-CASPT2/ANO-RCC-VTZP Relative Energies (kcal mol^{-1}) of Important Geometries Optimized at Various Levels of Theory

	$^1(\sigma,\sigma^*)$-Min	$^1(\sigma,\sigma^*)$-TS	$^1(n,\sigma^*)$-Min	$^1(n,\sigma^*)$-TS	$^3(n,\sigma^*)$-Min	$^3(n,\sigma^*)$-TS
MS-CASPT2 (with ZPE correction) //SA-CASSCF/ANO-RCC-VDZP	0.0	26.0	26.0	22.0	26.3	23.7
MS-CASPT2 //SA-CASSCF/ANO-RCC-VTZP	0.0	29.3	28.5	25.7	28.8	27.7
MS-CASPT2(10-in-7)[a] //SA-CASSCF(10-in-7)/ANO-RCC-VTZP	0.0	29.0	27.9	–	–	–
MS-CASPT2(18-in-15) //SA-CASSCF(16-in-13)/ANO-RCC-VDZP	0.0	26.9	–	–	–	–
direct MS-CASPT2 /ANO-RCC-VTZP optimization	0.0	27.0	26.1	–	–	–

[a] The (10-in-7) active space was produced by excluding the C_1-C_2 σ/σ^* orbitals and electrons from CAS(12-in-9) (see Chart 2). It is qualified only for calculating the S_0 activation energy, since the C−C bond is almost intact from **$^1(\sigma,\sigma^*)$-Min** to **$^1(\sigma,\sigma^*)$-TS**.

decreases to 26.0 kcal mol^{-1} (Table 2), which is in line with our previously calculated activation energy for 1,2-dioxetane (24.1 kcal mol^{-1} at the MS-CASPT2 level)[9] since the conjugation effect in dioxetanone strengthens the peroxide bond and consequently results in a higher dissociation barrier. At the same time, the theoretically predicted activation energy obtained here for the gas-phase decomposition of unsubstituted dioxetanone is higher than the experimentally measured E_a (∼22.3 ± 0.3 kcal mol^{-1}) of the dimethyl-substituted one in $C_2Cl_3F_3$ solution.[12] Although the theoretical results do not include solvent and substitution effects, the size of the difference called for an investigation of the stability of the theoretical results with respect to the model parameters. Hence, we reoptimized the structures at the SA-CASSCF level with alternative active spaces and the larger ANO-RCC-VTZP basis, and ultimately, some of the significant structures at the MS-CASPT2 level of theory (see Table 2). All of the calculations at various levels of theory showed identical characters for the ground-state minimum and transition state and provided relative energies that are consistent with each other.

3.2. The $^1(\sigma,\sigma^*)$-Min−TS-1−CI-1 MEP. The transition state **$^1(\sigma,\sigma^*)$-TS** of the ground-state PES was first located and verified by vibrational frequency analysis at the SA-CASSCF level. An imaginary frequency (756i cm^{-1}) corresponding to the stretching mode of the weak O_3-O_5 peroxide bond was found. The **$^1(\sigma,\sigma^*)$** MEP was established using the structure of **$^1(\sigma,\sigma^*)$-TS** as the starting geometry. Subsequently, the potential energy curves of the S_0, S_1, and T_1 states were calculated at MS-CASPT2 level of theory on the basis of the geometries along this part of the lowest-energy MEP. As illustrated in Figure 1, along the path **$^1(\sigma,\sigma^*)$-Min−$^1(\sigma,\sigma^*)$-TS**, the **$^1(\sigma,\sigma^*)$** and **$^1(n,\sigma^*)$** curves approach each other as the reaction advances toward the TS. At the first TS of the MEP, the MS-CASPT2 energy gap between

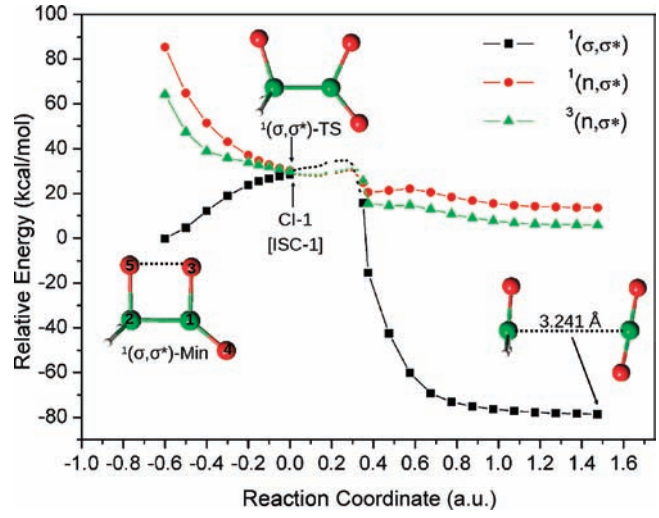

Figure 1. Computed MS-CASPT2//SA-CASSCF energy profile along the ground-state SA-CASSCF MEP [predominately **$^1(\sigma,\sigma^*)$**] in character] of dioxetanone. The dashed lines between reaction coordinates of 0.000 and 0.375 au illustrate the energy variation along the MEP while the **$^1(n,\sigma^*)$** state is the lowest-energy state.

the **$^1(\sigma,\sigma^*)$** and **$^1(n,\sigma^*)$** states is within 1.0 kcal mol^{-1}, implying either a possible crossing or, at least, a region where the considered adiabatic states strongly interact. Indeed, following the SA-CASSCF reaction path led to a conical intersection (**CI-1**, see Figure 1) slightly after **$^1(\sigma,\sigma^*)$-TS**. At the MS-CASPT2 level of theory, an energy gap of 0.6 kcal mol^{-1} between the two states was established (see Table 1).

The location of **CI-1** in the very close vicinity of **$^1(\sigma,\sigma^*)$-TS** governs the mechanism of the transition. Here the reactant has

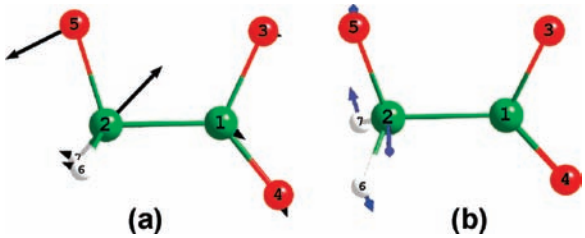

Figure 2. Calculated (a) in-plane (black arrows) and (b) out-of-plane (blue arrows) branching space vectors of CI-1.

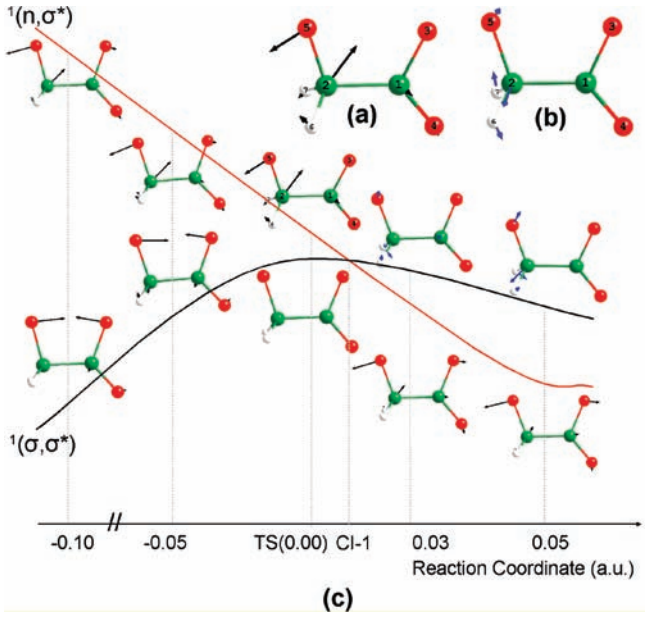

Figure 3. (a) In-plane molecular energy gradient vectors (black arrows) and (b) ones with out-of-plane components (blue arrows) at **CI-1**; (c) Molecular energy gradient vectors of selected structures on the schematic MEP around the CI.

negligible velocity in the direction of the reaction. Hence, the distribution of the wave packet in the two surfaces is not controlled by a Landau−Zener-like[20] mechanism. Rather the distribution is controlled by the population of the individual internal degree of freedom perpendicular to the reaction path.

The **CI-1** branching space vectors at the SA-CASSCF level of theory (illustrated in Figure 2) show an in-plane and an out-of-plane displacement character. Hence, the subsequent MEPs support either a planar or a nonplanar structure. Further analysis of the molecular energy gradients of the $^1(\sigma,\sigma^*)$ and $^1(n,\sigma^*)$ states using the structures along the lowest-energy-state MEP around **CI-1** (see Figure 3) revealed that the $^1(\sigma,\sigma^*)$ state supports a planar structure up to **CI-1**, after which this state has a bifurcation resulting from a twisting motion that would break the planar symmetry. That is, the MEP of this state does a sudden turn at or in the very close vicinity of **CI-1**. After **CI-1**, the $^1(n,\sigma^*)$ state, however, maintains a planar structure. The distribution of the wave packets on the two singlet PESs at **CI-1** is thus controlled by the distribution of the molecular vibrations and their relation to the branching space vectors.

3.3. The CI-1−$^1(n,\sigma^*)$-Min−CI-2−$^1(\sigma,\sigma^*)$-Product MEP. In the following analysis, we will selectively follow the MEP of the state of the lowest energy. This path preserves a planar structure. Along this path, the states of interest are close in energy. Following the excited-state surface MEP, which results in a nonplanar geometry, could be of interest; however, doing so lies beyond the scope of the current study.

From Figure 1, it is seen that along the $^1(n,\sigma^*)$ MEP after **CI-1**, the $^1(\sigma,\sigma^*)$ surface is slightly higher in energy than the $^1(n,\sigma^*)$ surface. Meanwhile, the energy gap between these two PESs remains within a few kilocalories per mole over an extended reaction-coordinate range (from 0.00 to 0.375 au, see Figure 1).

The energy profiles for the $^1(n,\sigma^*)$ and $^3(n,\sigma^*)$ excited states along the $^1(\sigma,\sigma^*)$ MEP are also shown in Figure 1. The $^3(n,\sigma^*)$ surface is essentially identical to that of $^1(n,\sigma^*)$, except that the former is lower in energy than the latter. Here spin−orbit coupling (SOC) is of significance in the population of the triplet state. In view of the accuracy of the current method, however, it would be a futile exercise to include SOC in the current analysis. The energetics at **CI-1** shows that the T_1 state is slightly above the S_0 state by 0.1 kcal mol^{-1}, which suggests the presence of an intersystem crossing (ISC) close to **CI-1** (**ISC-1**). Both the S_0/S_1 and S_0/T_1 pairs of surfaces intersect in the vicinity of $^1(\sigma,\sigma^*)$**-TS**, acting as one of the more interesting features of this reaction.

The intermediate on the $^1(n,\sigma^*)$ surface [$^1(n,\sigma^*)$**-Min**] presents a typical biradical nature in which the in-plane p orbital of O_3 and the perpendicular one of O_5 are singly occupied. The MS-CASPT2 energetic correction shows that $^1(n,\sigma^*)$**-Min** is 27.9 kcal mol^{-1} higher in energy than $^1(\sigma,\sigma^*)$**-Min** but is still slightly more stable than $^1(\sigma,\sigma^*)$**-TS** by 0.7 kcal mol^{-1}.

The $^1(n,\sigma^*)$ MEP starting from $^1(n,\sigma^*)$**-Min** and ending at a singlet excited formaldehyde and a ground-state CO_2 is straightforward. The transition state $^1(n,\sigma^*)$**-TS** (confirmed by the presence of only one imaginary frequency, 1272i cm^{-1}) corresponds to the breaking of the C−C bond. The low barrier height and exothermic properties suggest that $^1(n,\sigma^*)$**-Min** is thermodynamically unstable and instantly undergoes dissociation.

Table 1 and Figure 4 show that in some cases the MS-CASPT2//SA-CASSCF results do not closely match the SA-CASSCF//SA-CASSCF results. Because of the shallow nature of the PES, the stationary points on the SA-CASSCF and MS-CASPT2 PESs are not be identical. For instance, the maximum in the $^1(n,\sigma^*)$ MEP curve [denoted as $^1(n,\sigma^*)$**-TS′**] does not exactly correspond to the coordinate of $^1(n,\sigma^*)$**-TS**; instead, it lies 0.05 au earlier. Fortunately, the MS-CASPT2//SA-CASSCF approach did not significantly change the shapes and relative positions of the ground- and excited-state MEPs obtained at the SA-CASSCF level (Figure S1 in the Supporting Information), so it is still safe to interpret the SA-CASSCF reaction mechanism qualitatively and to some degree quantitatively. The relative energy (30.4 kcal mol^{-1}) of $^1(n,\sigma^*)$**-TS′** is 1.7 kcal mol^{-1} higher than that of the ground-state TS, $^1(\sigma,\sigma^*)$**-TS.** This suggests that the barrier for the generation of excited-state products is higher than the one for the decomposition of reactant. This finding supports the experimental results of Schmidt and Schuster.[12]

Figure 4b shows that the S_0/S_1 hypersurfaces intersect again shortly after $^1(n,\sigma^*)$**-TS′**, and therefore, the geometry of $^1(n,\sigma^*)$**-TS′** is also regarded as another crossing structure that is denoted as **CI-2** (or as **ISC-2** between the S_0/T_1 pair of surfaces). At the MS-CASPT2 level of theory, we find this conical intersection to be on a clearly more repulsive part of the PES. In this respect, one could expect that the reaction mechanism here is different from that observed at **TS-1/CI-1**. Notably, the frag-

(20) (a) Landau, L. D. *Phys. Sov. Union* **1932**, *2*, 46. (b) Zener, C. *Proc. R. Soc. London* **1932**, *A137*, 696.

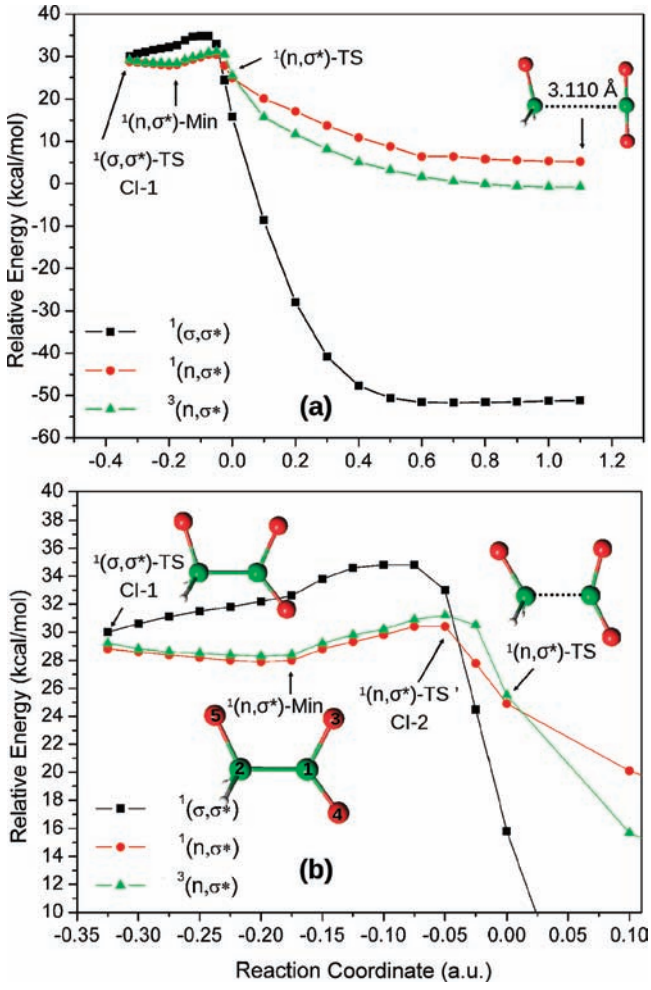

Figure 4. (a) Computed MS-CASPT2//SA-CASSCF energy profile. (b) Detailed view for the reaction-coordinate range from −0.35 to 0.10 au, along the ^{1}**(n,σ*)** MEP path from **CI-1** to ^{1}**(n,σ*)-Min** and the following the ^{1}**(n,σ*)** MEP.

mented nature of this TS/CI is much more subtle and governed by weaker interactions than **TS-1/CI-1**. Hence, the actual energetics and molecular structures at the SA-CASSCF and MS-CASPT2 levels of theory, as expected, were found to show larger deviations from each other than were observed for the earlier parts of the MEP. It should be noted that **CI-2** in some sense can be regarded as analogous to the reported minimum energy conical intersection (MECI) of firefly dioxetanone,[6d] except that **CI-2** represents a crossing structure located on the MEPs whereas the MECI is an optimized minimum in the crossing seam without any clear direct association to an MEP.

The details of the reaction mechanism, such as the formation of the excited-state product and the ratio of excited- to ground-state products, cannot be straightforwardly interpreted by a comparison of obtained barrier heights, even if they were precisely calculated. There are at least two more factors to be considered. First, there are two crossing points (CIs or ISCs), one located near ^{1}**(σ,σ*)-TS** and the other near ^{1}**(n,σ*)-TS′**, via which the molecules can repartition among the ground and excited states. Second, in the extended shallow basin where the ^{1}**(n,σ*)** surface is below the ^{1}**(σ,σ*)** state, the energy gap between them is less than 5.0 kcal mol^{-1}. This value is small enough to afford efficient nonadiabatic coupling (NAC). Therefore, the dissociation products should be not only controlled by the activation barriers for forming the corresponding species but also regulated by the cooperation of NAC effects. The biradical region, the part of the MEP from ^{1}**(σ,σ*)-TS** to ^{1}**(n,σ*)-TS**, represents another interesting feature of this reaction.

The ^{3}**(n,σ*)** MEP was found to be similar to that for ^{1}**(n,σ*)**. Along the triplet MEP, the geometries and energies of the minimum ^{3}**(n,σ*)-Min** and transition state ^{3}**(n,σ*)-TS** (with an imaginary frequency of 1411i cm^{-1}) as well as the shape of the curve are practically identical to those of the ^{1}**(n,σ*)** MEP, and thus, the energy profile along the ^{3}**(n,σ*)** MEP is depicted in Figure S2 in the Supporting Information without further discussion.

3.4. Reaction Coordinate Analysis and Suggested Mechanism. To analyze the reaction coordinate, it is useful to review that of the unsubstituted 1,2-dioxetane[9] to find similarities and differences. 1,2-Dioxetane undergoes either homolysis to form ground-state formaldehydes or heterolysis leading to ground- and excited-state products. During these processes, five coordinate modes are involved, including O−O′ and C−C′ bond stretching, O−C−C′−O′ torsion, asymmetric [O−C/O′−C′] bond stretching, and asymmetric [C/C′] pyramidalization. The case for dioxetanone is slightly different. First, along the excited-state pathways, only the formaldehyde molecule has a chance to be excited, while the carbon dioxide is always found in the ground state. Consequently, it is the C_2-O_5 bond stretching instead of the asymmetric [O−C/O′−C′] bond stretching that is involved in the reaction path. Second, unlike the out-of-plane O−C−C′−O′ mode in 1,2-dioxetane, which plays a role throughout the whole reaction path, the torsional mode around the C−C bond in dioxetanone was found to be in action only after **CI-1**.

According to the spatial geometric and gradient changes along the reaction path, the overall decomposition can be divided into three stages, which in short can be called the initial, biradical, and fragmented stages. In each stage, one or more modes play central roles in promoting the reaction forward.

(*i*) *The initial stage*. When the reactant is mildly heated, the thermolysis process is initiated. The O−O bond in the reactant is gradually elongated until the bond distance increases to 2.455 Å at ^{1}**(σ,σ*)-TS**. Meanwhile, the C−C bond remains intact throughout this process. As a result, biradical structure is formed. Figure 3 clearly shows that during this stage the gradient vectors of both the ground- and excited-state PESs are in-plane. More specifically, the vectors represent the O−O stretching mode as well as the C_2 pyramidalization mode.

(*ii*) *The biradical stage*. This stage corresponds to the state-interaction region discussed in the above subsections. It is a key stage in which reactive trajectories could be regulated among the S_0 and S_1 branches. At the entrance of this stage, the activated molecules in the ^{1}**(σ,σ*)** state start to be perturbed by the out-of-plane $O_3-C_1-C_2-O_5$ twisting mode while molecules in the ^{1}**(n,σ*)** state remain planar. The geometrical and gradient variations along the energetically favorable ^{1}**(n,σ*)** state MEP suggest this stage is also determined by the C_2 pyramidalization and C_2-O_5 bond stretching modes. As shown in Table 1 and Figure 5, the C_2 center in the ^{1}**(n,σ*)** branch shows more and more sp^3 character, with $C_1-C_2-O_5$ angles of 106.5, 114.6, and 119.2° in ^{1}**(σ,σ*)-TS**, ^{1}**(n,σ*)-Min**, and ^{1}**(n,σ*)-TS**, respectively. In addition, the C−C bond stretching also starts to play a role. Figure 5 shows that the variations of both the O−O and C−C distances in the ^{1}**(n,σ*)** state meet their inflection points near ^{1}**(n,σ*)-Min**, where the O−O distance ceases increasing while the C−C bond begins to elongate.

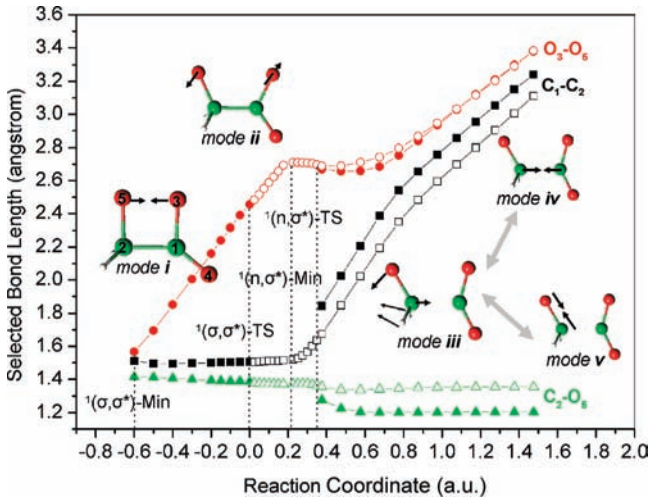

Figure 5. Variation of the C_1-C_2, O_3-O_5, and C_2-O_5 distances along the $^1(\sigma,\sigma^*)$ (solid symbols) and $^1(\mathbf{n},\sigma^*)$ (open symbols) MEPs. The representative modes include the (*i*) O−O stretching, (*ii*) O−C−C−O torsional, (*iii*) C_2 pyramidalization, (*iv*) C−C stretching, and (*v*) C_2-O_5 stretching modes.

(*iii*) *The fragmented stage*. In this final stage, the ground- and excited-state MEPs are separated in energy, and geometries on the ground-state branch exhibit longer C−C distances and shorter C_2-O_5 bond lengths than those on the excited one.

On the basis of the energy profiles and reaction mode analysis, a possible mechanism of the reaction can be outlined. Starting from the ground-state reactant, the system encounters the first intersection (**CI-1** or **ISC-1**) in the vicinity of $^1(\sigma,\sigma^*)$**-TS**. On one hand, the molecules intend to follow the direction of the in-plane branching vector and pass though the CI region to access the energetically favorable $^1(\mathbf{n},\sigma^*)$ state; on the other hand, a number of molecules are likely to follow the nonsymmetric $^1(\sigma,\sigma^*)$ branch at **CI-1** because of the contribution of the out-of-plane modes. Afterward, the molecules on the chemiluminescent branch are somewhat trapped by the shallow basin on the $^1(\mathbf{n},\sigma^*)$ surface. It is also possible that NAC effects are in action, given the narrow energy gap and the moderate structural difference between the S_0 and S_1 surfaces. The molecules are expected to redistribute among these branches until they are subjected to another hypersurface crossing (**CI-2** or **ISC-2**) shortly before $^1(\mathbf{n},\sigma^*)$**-TS**. Because of the difference between the SA-CASSCF and MS-CASPT2 methods, these crossing points are not exactly represented. The steeply downhill slopes on both surfaces in the proximity of **CI-2** (or **ISC-2**) suggest that a fast process is in action, and thus, the two structures might play a less important role in the state regulation. Accordingly, the $^1(\sigma,\sigma^*)$ trajectories proceed to form ground-state formaldehyde and those on the $^1(\mathbf{n},\sigma^*)$ surface go on to produce chemiluminescent products. As a whole, excited-state products are generated in a reasonably high quantum yield. However, on the basis of the current data, the triplet-to-singlet ratio cannot be rationalized. Although in theory a SOC calculation could be helpful, the subtle situation requires a treatment beyond the Born−Oppenheimer approximation and thus is beyond the ability of the currently employed quantum-chemistry codes. Moreover, since the SOC calculation heavily depends on the description of the balance between the singlet and triplet components, the extremely narrow gaps between these states will make any SOC calculation erratic and inconclusive.

Because of the subtle differences between the experimental results of Schmidt and Schuster[12] and those of Turro and Chow[13] as well as the shallow nature of the PESs at the TSs, no conclusive theoretical information in the present study can discriminate between the two experimental results. However, this study has conclusively demonstrated that the dissociation process is that of a classical two-step biradical mechanism. Theoretical evaluation of solvent and substitution effects on the decomposition of dioxetanone is in process. Further experimental work is suggested, such as precise experimental measurements on the gas-phase decomposition of unsubstituted dioxetanone, which would be helpful in rationalizing the evident discrepancy between experiment and theory, as well as a study of the photoinduced dissociation, which would reveal more information about the details of the PES around the points where the O−O and C−C bonds break.

4. Conclusions

In order to reveal the mechanistic details underlying the chemiluminescent decomposition of unsubstituted dioxetanone,

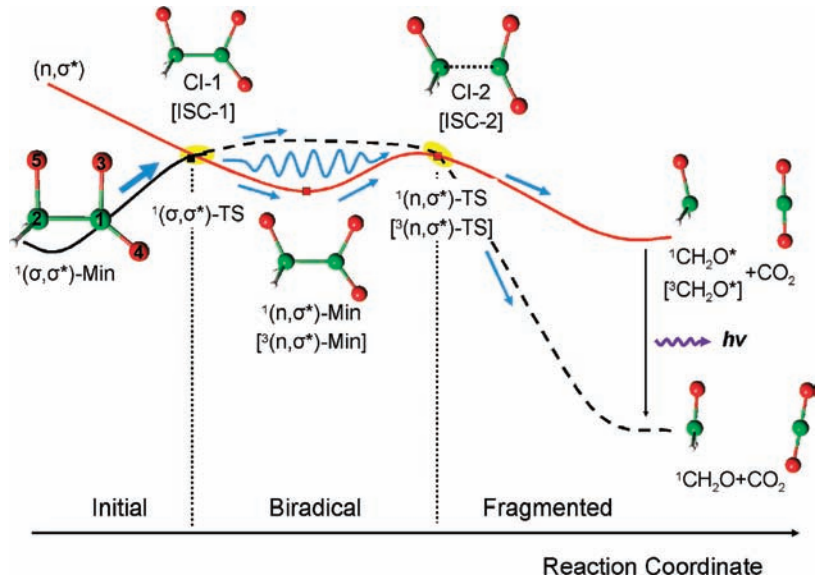

Figure 6. Schematic profile describing the mechanism of the chemiluminescent decomposition.

we have carried out MS-CASPT2//SA-CASSCF calculations on the S_0, S_1, and T_1 surfaces. Our results reveal some interesting features and suggest a possible mechanism. First of all, it is found that the chemiluminescent (or excited-state) branches of this nonadiabatic decomposition take place within the molecular plane, while the ground-state path bifurcates corresponding to a torsion of the O−C−C−O mode. This contrasts with the case of 1,2-dioxetane, in which the corresponding O−C−C−O mode was suggested to play a important role in the formation of excited-state formaldehyde. The second feature of the reaction is that there exists a particular biradical stage during the decomposition process during which the potential energy surfaces of the ground and excited states become close in energy and intersect twice along the reaction path (see Figure 6). This stage is responsible for the formation of the excited-state intermediates and the corresponding chemiluminescent products and is also expected to be in charge of regulating the reactive molecules among different reaction branches. The third feature is based on the previous one: because of the existence of this subtle stage, the overall quantum yields of the excited-state products are actually controlled by the cooperation of these effects instead of a simple comparison of the barrier heights on the ground- and excited-state branches. Finally, the following mechanism can be outlined (Figure 6): Molecules starting from the ground-state PES can access the **(n,σ^*)** surface via the crossings in the vicinity of the first transition state on the ground-state, generating the excited-state intermediates with reasonably high efficiency. Afterward, the trajectories on the S_0 and S_1 (or S_0 and T_1) surfaces have chances to be repartitioned in the extended basin around the excited-state intermediate until these pairs of states intersect again near the excited-state transition states. As a result, excited-state products are generated with particular quantum yields, after which the emission of light occurs during their subsequent decay to the ground state.

Acknowledgment. We thank the referees for their very valuable comments. This work was supported by the Swedish Science Research Council (VR) and Crafoordska Stiftelsen. Y.-J.L. acknowledges funding from the National Natural Science Foundation of China (Grants 20673012, 20873010, and 20720102038) and the Major State Basic Research Development Program (Grant 2007CB815206). The authors thank LUNARC Computer Center of Lund University and SNAC for granted computational time.

Supporting Information Available: Complete ref 18a, SA-CASSCF//SA-CASSCF and MS-CASPT2//SA-CASSCF energy profiles, and Cartesian coordinates for the structures involved in the reaction and their total and relative energies. This material is available free of charge via the Internet at http://pubs.acs.org.

JA808511T